

JGR Space Physics

TECHNICAL REPORTS: METHODS

10.1029/2021JA029700

Special Section:

Geospace multi-point observations in Van Allen Probes and Arase era

Key Points:

- Measurements of electromagnetic waves on Van Allen Probes and Arase are inter-calibrated with intense whistlers during a close conjunction
- Magnetic search coil measurements are the same within 14%, polarization and propagation parameters are consistent, timing is within 10 ms
- Electric field amplitudes match within 33% when we include the newest results on antenna-plasma interface with measured plasma densities

Correspondence to:

O. Santolik,
os@ufa.cas.cz

Citation:

Santolik, O., Miyoshi, Y., Kolmašová, I., Matsuda, S., Hospodarsky, G. B., Hartley, D. P., et al. (2021). Inter-calibrated measurements of intense whistlers by Arase and Van Allen Probes. *Journal of Geophysical Research: Space Physics*, 126, e2021JA029700. <https://doi.org/10.1029/2021JA029700>

Received 21 JUN 2021
Accepted 17 AUG 2021

© 2021. The Authors.

This is an open access article under the terms of the [Creative Commons Attribution-NonCommercial-NoDerivs License](#), which permits use and distribution in any medium, provided the original work is properly cited, the use is non-commercial and no modifications or adaptations are made.

Inter-Calibrated Measurements of Intense Whistlers by Arase and Van Allen Probes

O. Santolik^{1,2} , Y. Miyoshi³ , I. Kolmašová^{1,2} , S. Matsuda⁴ , G. B. Hospodarsky⁵ , D. P. Hartley⁵ , Y. Kasahara⁶ , H. Kojima⁷ , A. Matsuoka⁸ , I. Shinohara⁴ , W. S. Kurth⁵ , and C. A. Kletzing⁵ 

¹Department of Space Physics, Institute of Atmospheric Physics of the Czech Academy of Sciences, Prague, Czechia, ²Faculty of Mathematics and Physics, Charles University, Prague, Czechia, ³Institute for Space-Earth Environmental Research, Nagoya University, Nagoya, Japan, ⁴Institute of Space and Astronautical Science, Japan Aerospace Exploration Agency, Sagami-hara, Kanagawa, Japan, ⁵Department of Physics and Astronomy, University of Iowa, Iowa City, IA, USA, ⁶Graduate School of Natural Science and Technology, Kanazawa University, Kanazawa, Ishikawa, Japan, ⁷Research Institute for Sustainable Humanosphere, Kyoto University, Uji, Kyoto, Japan, ⁸Data Analysis Center for Geomagnetism and Space Magnetism, Graduate School of Science, Kyoto University, Kyoto, Japan

Abstract Measurements of electromagnetic waves in space plasmas are an important tool for our understanding of physical processes in this environment. Inter-calibration of data from different spacecraft missions is necessary for combining their measurements in empirical models or case studies. We show results collected during a close conjunction of the Van Allen Probes and Arase spacecraft. The inter-calibration is based on a fortuitous case of common observations of strong whistlers at frequencies between a few hundred hertz and 10 kHz, which are generated by the same lightning strokes and which propagate along very similar paths to the two spacecraft. Measured amplitudes of the magnetic field fluctuations are the same within ~14% precision of our analysis, corresponding to 1.2 dB. Currently, archived electric field measurements show twice larger amplitudes on Arase compared to Van Allen Probes but they start to match within ~33% precision (2.5 dB) once the newest results on the interface of the antennas to the surrounding plasma are included in the calibration procedures. Ray tracing simulations help us to build a consistent scenario of wave propagation to both spacecraft reflected by a successful inter-calibration of the polarization and propagation parameters obtained from multicomponent measurements. We succeed in linking the spacecraft observations to localizations of lightning return strokes by two different ground-based networks which independently verify the correctness of the Universal Time tags of waveform measurements by both spacecraft missions, with an uncertainty better than 10 ms.

1. Introduction

Direct in situ measurements of electromagnetic waves in space plasmas are crucial for explaining physical processes not only in the plasma environment of the Earth (D. Gurnett et al., 1966; Mosier & Gurnett, 1969), including the important region of the Van Allen belts (Horne et al., 2005; Thorne et al., 2013), but also in the environments of planets in the Solar System (D. Gurnett et al., 1996, 1981, 1983) and in the interplanetary space (D. Gurnett & Kurth, 2008). Modern instrumentation designed for these measurements often includes multicomponent measurements, usually composed of tri-axial magnetic search coil sensors and two or three electric antennas. Long electric antennas are used in the spin plane of spin-stabilized spacecraft while the electric field component along the spin axis is measured by shorter antennas or not measured at all. The receivers are designed to yield data on intensity, polarization, and propagation properties of the observed waves.

Examples of recent or current spacecraft missions with these capabilities include the Plasma wave instrument on the Polar spacecraft (D. A. Gurnett et al., 1995), the Spatio-Temporal Analysis of Field Fluctuations instrument on the Cluster spacecraft (Cornilleau-Wehrlin et al., 1997; Cornilleau-Wehrlin et al., 2003), FIELDS instrument on the Magnetospheric Multi-scale spacecraft (Torbert et al., 2016), the Search Coil Magnetometer and Electric Field Instrument on the Time History of Events and Macroscale Interactions during Substorms spacecraft (Roux et al., 2008; Bonnell et al., 2008), the Electric and Magnetic Field Instrument

Suite and Integrated Science (EMFISIS) Waves instrument on Van Allen Probes (Kletzing et al., 2013), and the Wave Form Capture (WFC) of Plasma Wave Experiment (PWE) with the Magnetic Field Experiment (MGF) onboard the Arase spacecraft (Kasahara et al., 2018; Matsuda et al., 2018; Matsuoka, Teramoto, Nomura, et al., 2018; Miyoshi, Shinohara, & Jun, 2018).

All these instruments were carefully calibrated before the launch but the space environment is different from the laboratory conditions, and some calibration activities can only be done while in flight. The instruments are also very sensitive and their performance can degrade with time in orbit. Therefore, in-flight inter-calibration between different missions are needed to ensure consistent results, especially if data from different missions are combined to build empirical models for space weather applications (e.g., Meredith et al., 2018), or if common measurements are used in case studies.

As a recent example, following the first results of Santolik et al. (2018) for another chorus case, Colpitts et al. (2020) showed conjugate observations of very weak whistler mode chorus observed by Arase PWE instrument and EFW instrument on Van Allen Probes during a close conjunction of the two spacecraft on August 21, 2017. Based on their results, comparison of measured amplitudes at Arase with Van Allen Probe B is impossible, as uncalibrated data in arbitrary units were used. Comparison with Van Allen Probe A in their Figure 4 shows very different power spectral densities on the two spacecraft reaching ~ 0.1 pT²/Hz for EFW on Van Allen Probe A and only $\sim 5 \times 10^{-4}$ pT²/Hz for PWE on Arase. This intriguing measurement clearly demonstrates the usefulness of the inter-calibration of the two instruments.

The in-flight inter-calibration becomes possible when the two spacecraft are at very close separations, ideally comparable to the wavelength of the measured waves. This is rarely possible, taking into account that, for example, the typical wavelengths at frequencies of hundreds of hertz to several kilohertz can be on the order of units to tens of km. Spacecraft orbits usually exclude such extremely close conjunctions and we, therefore, should not always expect an exact match of their measurements when they approach to separations of hundreds or thousands of wavelengths. Even in such a situation, the inter-calibration can be done if the measured waves propagate to the two spacecraft from the same source and if their propagation paths are reasonably similar.

In this article, we describe such an event when Van Allen Probes are in a close conjunction with Arase, and both the EMFISIS Waves instrument on Van Allen Probes and the Plasma Wave Experiment on Arase detect intense whistlers generated from the same lightning strokes and having propagated along approximately the same path to the two spacecraft. In Section 2, we describe the instrumentation, the data selection procedure, and we introduce the analyzed event. Section 3 brings an overview of wave observations during the relevant part of the Van Allen Probes orbit based on the survey mode data set and describes the analysis techniques. In Section 4, we show results based on the burst mode waveform data sets of Van Allen Probes and Arase. Section 5 is devoted to determination of the source lightning strokes, using ground-based networks, and to a discussion based on ray tracing simulations, Section 6 discusses the electric field measurements, and, finally, Section 7 briefly summarizes the results and their consequences for future work.

2. Data

The EMFISIS Waves instrument onboard the Van Allen Probes (Kletzing et al., 2013) measures three orthogonal magnetic field components by search coil sensors, two electric field components in the spin plane by two double probe antennas having lengths of 100 m tip to tip, and a spin axis electric field component using a 14 m long antenna. The resulting six-dimensional signals are sampled at 35 kHz and recorded by a six-channel waveform receiver (WFR) in various possible instrument modes. The maximum duration of continuously recorded snapshots is 5.968 s with a 32 ms gap between successive captures during the Continuous Waveform Burst mode intervals.

The sampled six-dimensional signals are also processed onboard by a Fast Fourier Transform (FFT) procedure based on 0.468 s long waveform snapshots repeated every 6 s. The resulting complex spectra are processed onboard to form averaged Hermitian spectral matrices 6×6 in 65 approximately logarithmically distributed frequency bins between 2 Hz and 12 kHz, with the increasing number of averaged matrices at higher frequencies and no averaging below 30 Hz. Additionally, a single electric field component is recorded

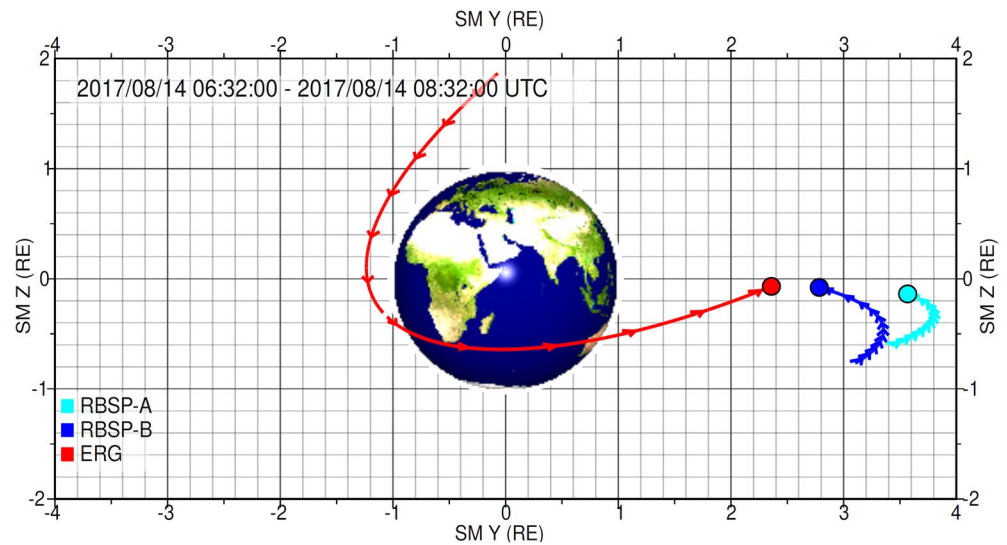


Figure 1. Projections of orbits of the Van Allen Probes A and B (shown by cyan and blue lines, respectively, as RBSP-A and RBSP-B), and Arase (shown by a red line as ERG) onto a Z-Y plane of the solar magnetospheric coordinates. The plot corresponds to a time interval of 2 h, with arrows plotted along the orbits with an interval of 10 min, and with color-coded circles showing the final position of the three spacecraft at 8:32 UT on August 14, 2017.

by a high-frequency receiver in a frequency range of 10–500 kHz. This measurement is used to determine the plasma density (Kurth et al., 2015) from the measured upper hybrid resonance frequency and the ambient magnetic field strength measured by the EMFISIS fluxgate magnetometer.

The PWE instrument onboard the Arase spacecraft (Kasahara et al., 2018) measures three orthogonal magnetic field components by search coil sensors, and two electric field components in the spacecraft spin plane by two double probe antennas, which have a length of 32 m tip to tip (Kasaba et al., 2017). From the various data products of this instrument, we have selected the data of the waveform capture receiver which records waveforms of two electric and three magnetic field components with a sampling frequency of 65,536 Hz. The burst mode of this receiver can yield continuous waveforms with a duration of 8–200 s (Matsuda et al., 2018). These waveforms from PWE/WFC onboard Arase can be analyzed using ISEE_3D that is an interactive plasma wave analysis tool (Matsuda, Miyoshi, et al., 2021). The characteristics of the antenna impedance of Arase using the in situ measurements have been reported by Matsuda, Kojima, et al. (2021).

For the inter-calibration of the EMFISIS Waves instrument onboard the Van Allen Probes and the PWE instrument onboard Arase, we have selected observations of lightning generated whistlers (Storey, 1953), as they usually propagate as planar waves and their propagation is easier to analyze compared to linear or nonlinear wave emissions of whistler mode hiss or chorus generated by plasma instabilities in the magnetosphere. We have used a list of 69 close conjunctions of the two spacecraft between June 13, and December 30, 2017 and we have selected cases, where the high cadence waveforms of electric and magnetic field fluctuations were measured by both instruments at the same time and where the waveform records contained intense whistlers. We have excluded cases where separate whistlers followed each other very rapidly, so that it would be difficult to identify the source lightning discharges. We have also excluded cases with diffuse whistler traces for which the dispersion would not be well defined. This procedure resulted in a down selection of six candidate cases from which we have selected the observations recorded on August 14, 2017 for our inter-calibration analysis.

Figure 1 shows projections of parts of orbits of the Arase and Van Allen Probes spacecraft on the Y-Z plane of the solar magnetospheric coordinates, together with the position of the three spacecraft at 8:32 UT on August 14, 2017. At that time the three spacecraft were located close to the geomagnetic equator at slightly different radial distances ranging from 2.65 Earth radii (R_E) for Arase, through 2.85 R_E for Van Allen Probe B, to 3.89 R_E for Van Allen Probe A. The spacecraft was located in the afternoon sector, at very similar magnetic local times of 16.3, 17.1, and 16.4 h for Arase, Van Allen Probe B, and Van Allen Probe A, respectively.

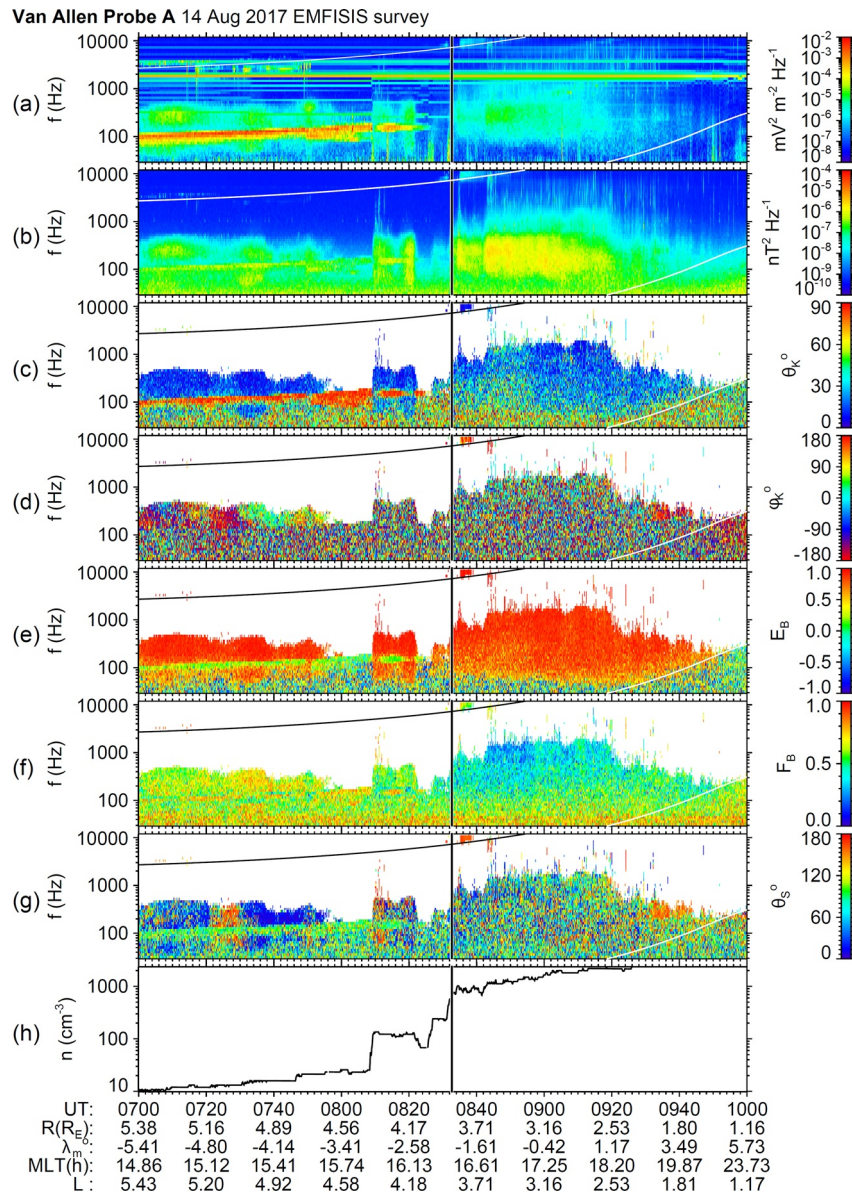


Figure 2. Results of analysis of the survey mode data of the EMFISIS Waves instrument onboard the Van Allen Probe A spacecraft between 7:00 and 10:00 UT on August 14, 2017. (a) Total power spectral density of electric field fluctuations obtained as the trace of the electric spectral matrix 3×3 ; (b) total power spectral density of magnetic field fluctuations obtained as the trace of the magnetic spectral matrix 3×3 ; (c) angle between the wave vector and the vector of the background magnetic field; (d) azimuth of the wave vector measured from the outward direction in the plane of the local magnetic meridian (e) signed ellipticity of the magnetic field polarization; (f) planarity of the magnetic field polarization; (g) angle between the spectral estimate of the Poynting vector and the vector of the background magnetic field; (h) plasma density obtained from the upper hybrid resonance frequency. Proton cyclotron frequency and one half of the electron cyclotron frequency are over plotted in panels (a–g). Vertical black line indicates the interval selected for the waveform analysis in Section 4.

3. Overview of Observations

Figure 2 presents an overview of 3 h of observations of the EMFISIS instrument on Van Allen Probe A, centered at 8:32 UT on August 14, 2017. We have analyzed the survey mode spectral matrices in order to determine not only the amplitudes of the observed electromagnetic waves but also their polarization and propagation properties. The total power spectral density of the electric field fluctuations (Figure 2a) has been obtained as the sum of the three power spectral densities obtained from the three orthogonal electric

antennas. A similar procedure has been used for the total power spectral density of the magnetic field fluctuations in Figure 2b.

The direction of the wave vector has been characterized by two spherical angles (Figures 2c and 2d): θ_k represents the angle between the wave vector and the vector of the background magnetic field obtained from the EMFISIS fluxgate magnetometer, while φ_k characterizes the azimuth of the wave vector with respect to the background magnetic field. We have used the singular value decomposition (SVD) technique (Santolík et al., 2003) to obtain these angles. The same technique has been used for the estimator F_B of the planarity of magnetic field fluctuations (Figure 2f), representing a measure of the validity of the assumption of the presence of a single plane wave. We have used a similar SVD technique to estimate the signed ellipticity E_B of the magnetic field fluctuations in Figure 2e (Santolík et al., 2002). The angle θ_s between the Poynting vector and the vector of the background magnetic field (Figure 2g) has been obtained by a spectral technique (Santolík et al., 2010). Finally, the plasma density in Figure 2h has been estimated from the observed upper hybrid resonance frequency and the background magnetic field strength (Kurth et al., 2015).

Van Allen Probe A moved from the apogee of its orbit to its perigee during the interval presented in Figure 2, with globally increasing plasma density from the plasma trough to the plasmasphere. The character of the observed electromagnetic waves also changed during this transition. In the first half of the interval, we observe a combination of right hand polarized exohiss at several hundreds of Hz propagating parallel to the magnetic field lines mostly toward the geomagnetic equator, with linearly polarized equatorial noise having wave vectors perpendicular to the local field line. Properties of both types of waves are consistent with their propagation in the cold plasma whistler mode. In the high plasma density region during the second half of the analyzed interval, we often observe short bursts of right-hand polarized waves which correspond to lightning-generated whistlers. They propagate from both the northern and southern hemispheres, often with wave vectors at small angles from the local background field line.

Figure 3 shows results from the same time interval but obtained by Van Allen Probe B, which dives sooner into the dense plasmaspheric region than Van Allen Probe A. Nevertheless, the detected types of electromagnetic waves, their polarization, and propagation properties remain the same. This especially includes observations of similar signatures of intense lightning generated whistlers, which occur on Van Allen Probe B already after 8:00 UT.

4. Conjugate Measurements by Arase and Van Allen Probes

Figure 4 presents an example of results of a detailed analysis of the continuous waveform data captured by Van Allen Probe B in this region, showing an interval of 3 s from 08:32:37 UT on August 14, 2017. Data from the shorter spin axis electric antenna are not used in the analysis, in order to avoid interferences and interpretation issues linked to this antenna. Signals from three magnetic antennas and two spin plane electric antennas are analyzed by a 512 point FFT, yielding a frequency resolution of 68.4 Hz. The data segments are overlapped by 90% of their duration before the analysis, allowing thus for smoother results as a function of time. Resulting spectral matrices are then analyzed by the same methods as the survey mode data in Figure 2.

Spectrograms in Figures 4a and 4b show a pair of intense whistlers arriving with a mutual time separation of ~ 60 ms around 08:32:37.700 UT and dispersing to lower frequencies for the following 900 ms, while always keeping the same mutual time separation. The whistlers are followed by a hissy intensification about 1 s later (marked as “R1”) and by a weaker hiss interval after another 1 s (marked as “R2”). The whistlers propagate at small angles of 15° – 30° from the local magnetic field line (Figure 4c), with wave vectors slightly inclined outward from the Earth (Figure 4d), while the hiss intervals contain waves propagating at high wave vector angles (e.g., Hartley et al., 2018).

The analysis techniques that we use for obtaining the wave vector directions are based on the determination of the normal direction to the plane of polarization of the magnetic field fluctuations (Santolík et al., 2003). The results, therefore, do not distinguish between two antiparallel possibilities for the normal directions and assume that the magnetic field fluctuations are well confined in a single plane. High planarities (Figure 4f) of the whistlers and of initial parts of the hiss intervals validate this hypothesis, and, as we can expect

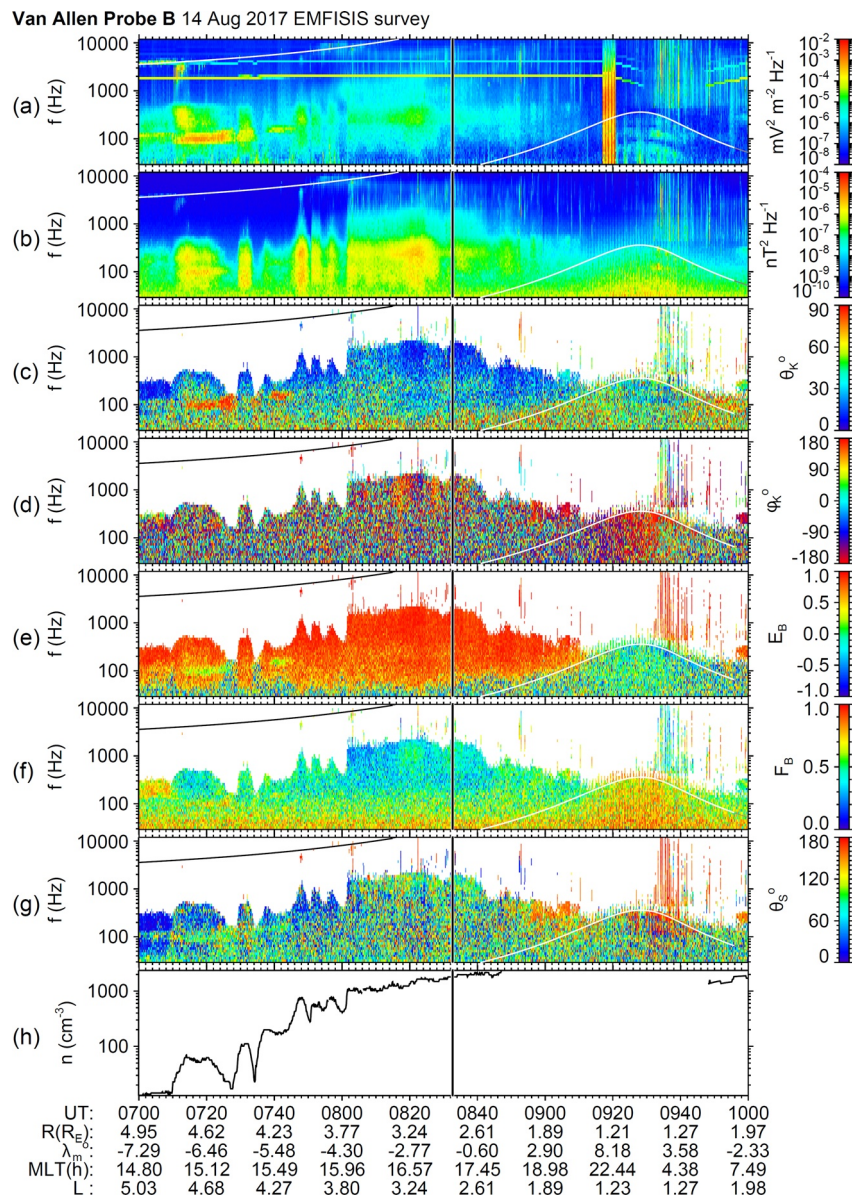


Figure 3. The same as in Figure 2 but for the survey mode data of the EMFISIS Waves instrument onboard the Van Allen Probe B spacecraft. Note that the intensification feature in panel (a) near 9:20 UT is an artifact with no physical relevance.

in the analyzed frequency range, all these waves also propagate in the right hand polarized whistler mode (Figure 4e), as shown by ellipticity ~ 1 .

Obtained spectral estimates of the direction of the Poynting vector (Figure 4g) can be used to determine the direction of wave propagation without ambiguity. In this case, when we do not use the direct measurements along the spin axis antenna, the third electric field component is calculated from measurements of the two electric antennas and three magnetic antennas using the Faraday's law in the spectral domain (Santolík et al., 2003). The results indicate that whistlers came to the equator from the southern hemisphere with the Poynting vectors nearly parallel to the direction of the background magnetic field, while the hiss interval "R1" came from the northern hemisphere, being most probably triggered by the first magnetospheric reflection of the original whistlers. The weaker hiss interval "R2" then probably corresponds to the second reflection on the south from the spacecraft position.

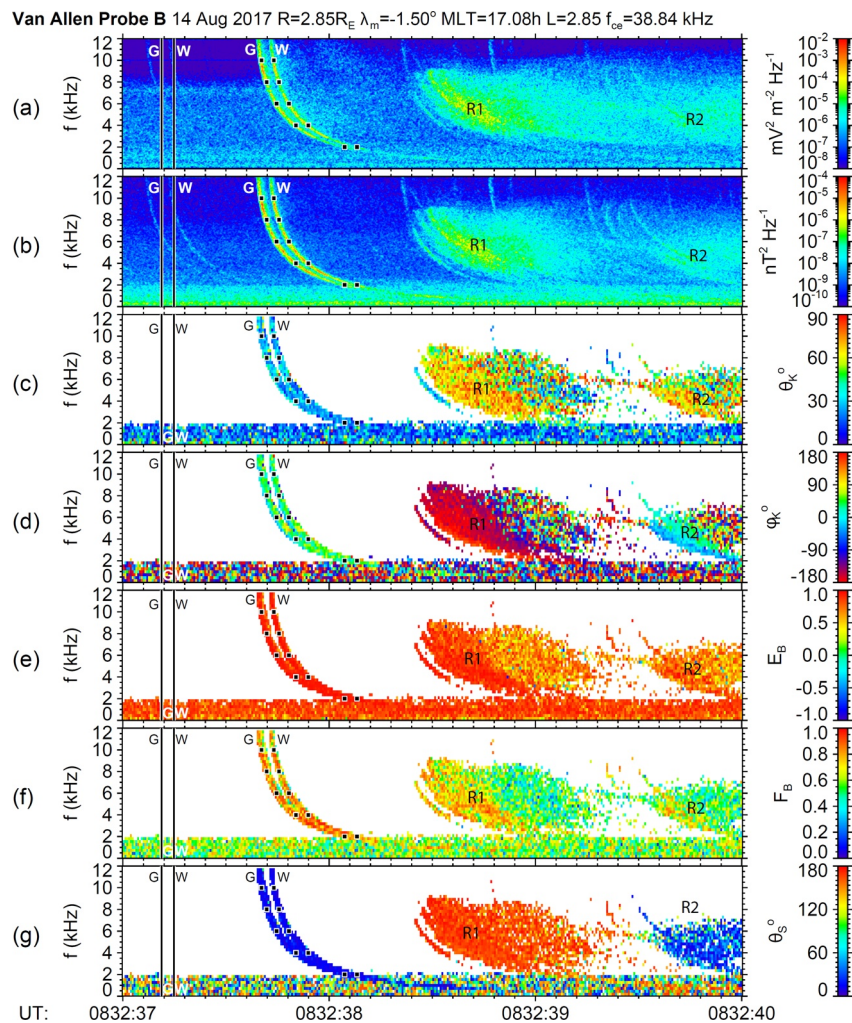


Figure 4. Results of analysis of the continuous burst mode data recorded in the frequency band below 12 kHz by the EMFISIS instrument onboard the Van Allen Probe B on August 14, 2017 during 3 s from 08:32:37 UT. The same quantities as in panels (a–g) of Figure 2 but based on spectral analysis of waveform records, and with only two spin-plane electric field antennas in panel a. Time of the source lightning return strokes detected by ground-based lightning detection networks GLD 300 (G) and WWLLN (W) (see Section 5) is indicated by black vertical lines. The resulting group times from ray-tracing analysis at frequencies of 2, 4, 6, 8, and 10 kHz are indicated by black squares for both lightning strokes G and W. Magnetospheric reflections are annotated by “R1” and “R2”.

As the pair of intense whistlers propagates below one half of the electron cyclotron frequency with wave vectors that are only slightly inclined from the local magnetic field line outward from the Earth (Figures 4c and 4d) and well below the Gendrin angle, we can expect a source at magnetic field lines which are slightly closer to the Earth than Van Allen Probe B. It would therefore be surprising to detect a similarly strong pair of whistlers on Van Allen Probe A, which is located even further out from the Earth at radial distances of more than one Earth radius larger. Indeed, Figure 5 shows only extremely weak pair of whistlers on Van Allen Probe A but with the same distinct time separation as on Van Allen Probe B. However, the frequency interval is limited and dispersion is very different owing to the propagation in a weaker background magnetic field at larger radial distances. Polarization and propagation analysis by the same methods as in Figure 4 again reveals right hand polarized whistler mode waves propagating from the southern hemisphere, this time at larger angles of the wave vectors from the local magnetic field line. The large separation distance between the two spacecraft does not allow any comparison between their measurements nor inter-calibration of Van Allen Probe A and Arase.

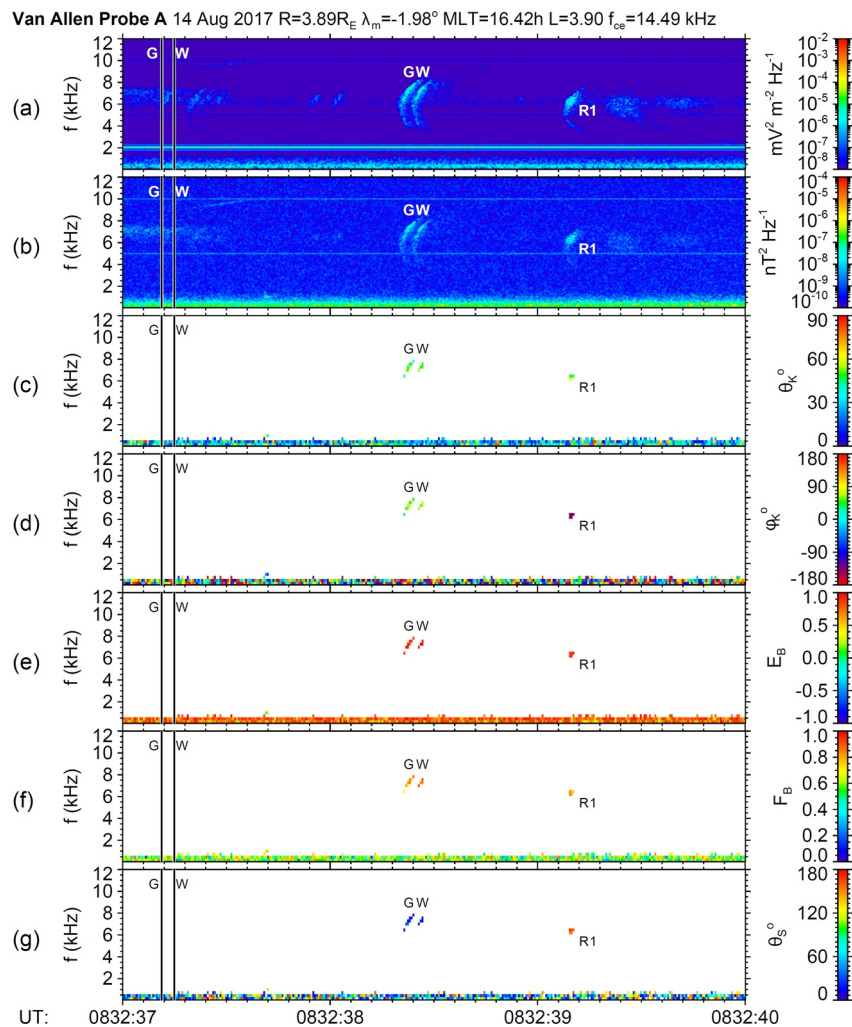


Figure 5. The same as in Figure 4 but for the continuous burst mode data recorded by the EMFISIS instrument onboard the Van Allen Probe A.

Fortuitously, Van Allen Probe B and Arase are at much lower separations at that time, Arase being closer to the Earth where we can expect the source magnetic field lines for the observed whistlers. Figure 6 shows results of analysis of the waveform data from the PWE instrument onboard the Arase spacecraft. We have used the same time interval and the same analysis techniques as in Figure 4. The observations are very similar to the results from the Van Allen Probe B. The two whistlers arrive only slightly (by ~40 ms) later but with the same characteristic time separation of 60 ms, and the hiss intervals “R1” and “R2” are also detected. We observe the same pattern of Poynting vector directions in Figure 4g.

Polarization properties in Figures 6e and 6f are also very similar to the results from Van Allen Probe B shown in Figures 4e and 4f, respectively. Significant differences are only obtained for wave vector directions in Figures 6c and 6d, compared to results in Figures 4c and 4d. On Arase, wave vectors are at a larger angle from the local magnetic field, reaching 35°–50° and, noticeably, they are inclined in the direction inward to the Earth. This means that, on Arase and Van Allen Probe B, the wave vectors are found on the opposite sides of the local magnetic field line in the plane of the local magnetic meridian.

In spite of the differences in the obtained wave vector directions, it is very likely that Arase and Van Allen Probe B recorded electromagnetic waves coming from the same lightning sources. As the two spacecraft are in a close conjunction we can also expect that the detected whistlers propagated along reasonably similar paths (see a discussion below) and that they should have approximately the same intensities of their electric

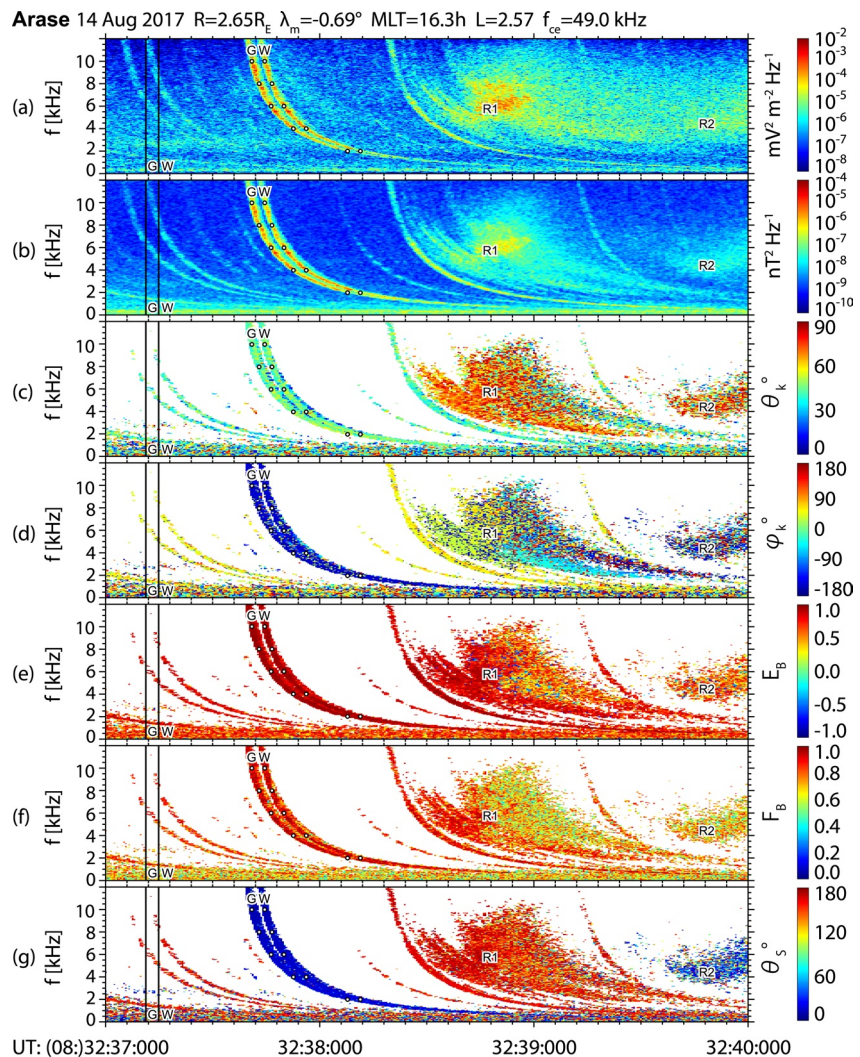


Figure 6. The same quantities as in Figure 4 but calculated from measurements of the PWE instrument on board the Arase satellite during the same time interval.

field and magnetic field fluctuations. The recorded data can be therefore used for the inter-calibration of the two data sets. Figure 7 shows the line plots of the average power spectral densities during the time intervals of Figures 4 and 6. We have used a frequency band from 5.5 to 6.5 kHz. The results in Figure 7a shows that Arase detects approximately 4 times (by 6 dB) larger electric field power spectral densities of the observed whistlers compared to Van Allen Probe B. This corresponds to twice larger electric field amplitudes on Arase. Figure 7b demonstrates that measurements by the tri-axial magnetic field search coil sensors give very similar results on the two spacecraft. The magnetic field power spectral densities match within 30% (1.2 dB), corresponding to 14% for the measured magnetic field amplitudes.

5. Discussion on the Differences of Obtained Wave Vector Directions: Source Lightning Strokes and Backward Ray Tracing Simulation

Knowing now that the source lightning discharges for both whistlers must be located in the southern hemisphere, we can verify if these lightning strokes exist in the records of ground-based lightning location networks. We also know that the whistlers propagate at frequencies below one half of the electron cyclotron frequency with wave vectors at small angles from the local magnetic field line. We can therefore expect that they propagate in a magnetospheric duct with an increased density near the magnetic field lines passing

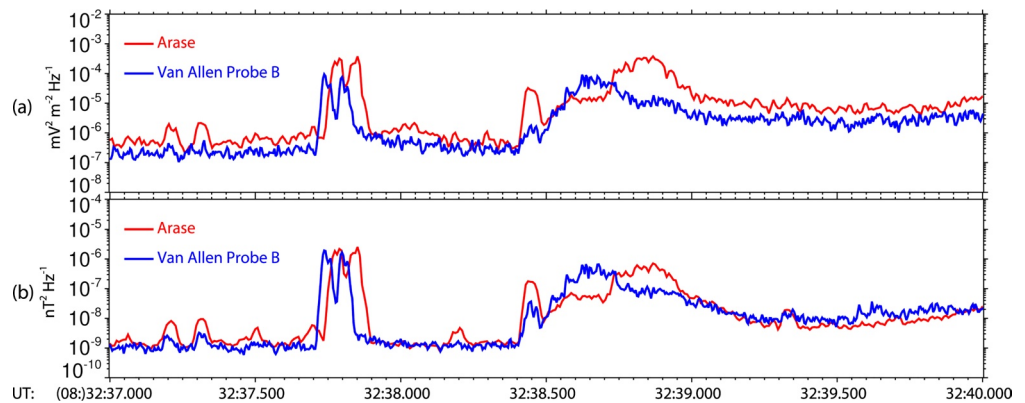


Figure 7. Comparison of the power spectral densities from (red) Arase PWE instrument, and (blue) Van Allen Probe B EMFISIS Waves instrument. Average power spectral density has been calculated in a 1 kHz band centered at 6 kHz, within the time intervals of Figures 4 and 6, from (a) measurements of two spin plane electric antennas; (b) measurements of the three orthogonal search coil antennas.

through the two spacecraft. We have searched the area within 2,000 km around the spacecraft geomagnetic foot points in the southern hemisphere. These locations for the Van Allen Probe B and Arase spacecraft are respectively found at geographical coordinates 40.9°S, 128.7°E and 39.0°S, 119.4°E, both being situated in the Indian Ocean, close to the southern coast of Australia.

We have found a strong negative return stroke with a peak current of -134 kA in the Global Lightning Data set GLD360 (Rudlosky et al., 2017; Said et al., 2010). This stroke was localized very close to the Van Allen Probe B footprint, at geographical coordinates 40.5°S, 130.6°E (approximately 1,000 km southwest from Adelaide, Australia), and occurred at 08:32:37.188 UT, as it is marked by a vertical line with the letter “G” in Figures 4–6. Sixty milliseconds later, at 08:32:37.248 UT, another strong lightning discharge with an equivalent peak current of 205 kA (Hutchins, Holzworth, Brundell, et al., 2012; Hutchins, Holzworth, Rodger, et al., 2012) was again detected at a very close location, 40.4°S, 130.6°E, by the World Wide Lightning Location Network (WWLN). The time of this second stroke is marked by a vertical line with the letter “W” in Figures 4–6. The same letters are then used also to mark the whistler traces corresponding to these two strokes. Interestingly, none of the two networks detected both strokes, probably owing to the disturbing presence of saturated waveforms, strong ionospheric reflections, or radiation from recoil leaders (Cummins, 2000) recorded by separate stations of the network in connection with these strong discharges. Such complex signals may sometimes cause difficulties to automated detection procedures developed for operational lightning location service.

With the known time of the source lightning, we can not only validate our assumptions on propagation of whistlers but also independently verify the onboard time tagging for the two spacecraft. Whistlers are traditionally analyzed by calculating their dispersion coefficient from the observed time delays at different frequencies, assuming that the group speed linearly increases as a function of the square root of frequency. This assumption is only valid for frequencies much lower than the frequency of the local maximum of the group velocity, which is at one quarter of the electron cyclotron frequency. In our case, the whistler frequencies exceed safe limits of this assumption and a more complex approach is necessary. We have therefore used a backward ray-tracing simulation procedure based on an earlier technique of Cerisier (1970) with a dipole magnetic field model and a diffusive equilibrium model of the plasma density distribution. The procedure includes an additional adaptive integration step algorithm with verification of the Wentzel-Kramers-Brillouin (WKB) approximation of the geometric optics (Santolík et al., 2006, 2009).

The diffusive equilibrium plasma density model is necessarily only a crude representation of the real distribution but it is sufficient to demonstrate the observed effects after some adjustments: we have arbitrarily added a small field-aligned duct, characterized by a 5% increase of the plasma density over a width of 0.1 Earth radii centered on a magnetic field line at $L = 2.8$. This duct is located between Arase at $L = 2.57$ and Van Allen Probe B at $L = 2.85$. Such a small density variation is well below the resolution limits of at least 10% for the method of Kurth et al. (2015) and thus it is not observable experimentally. However, it is

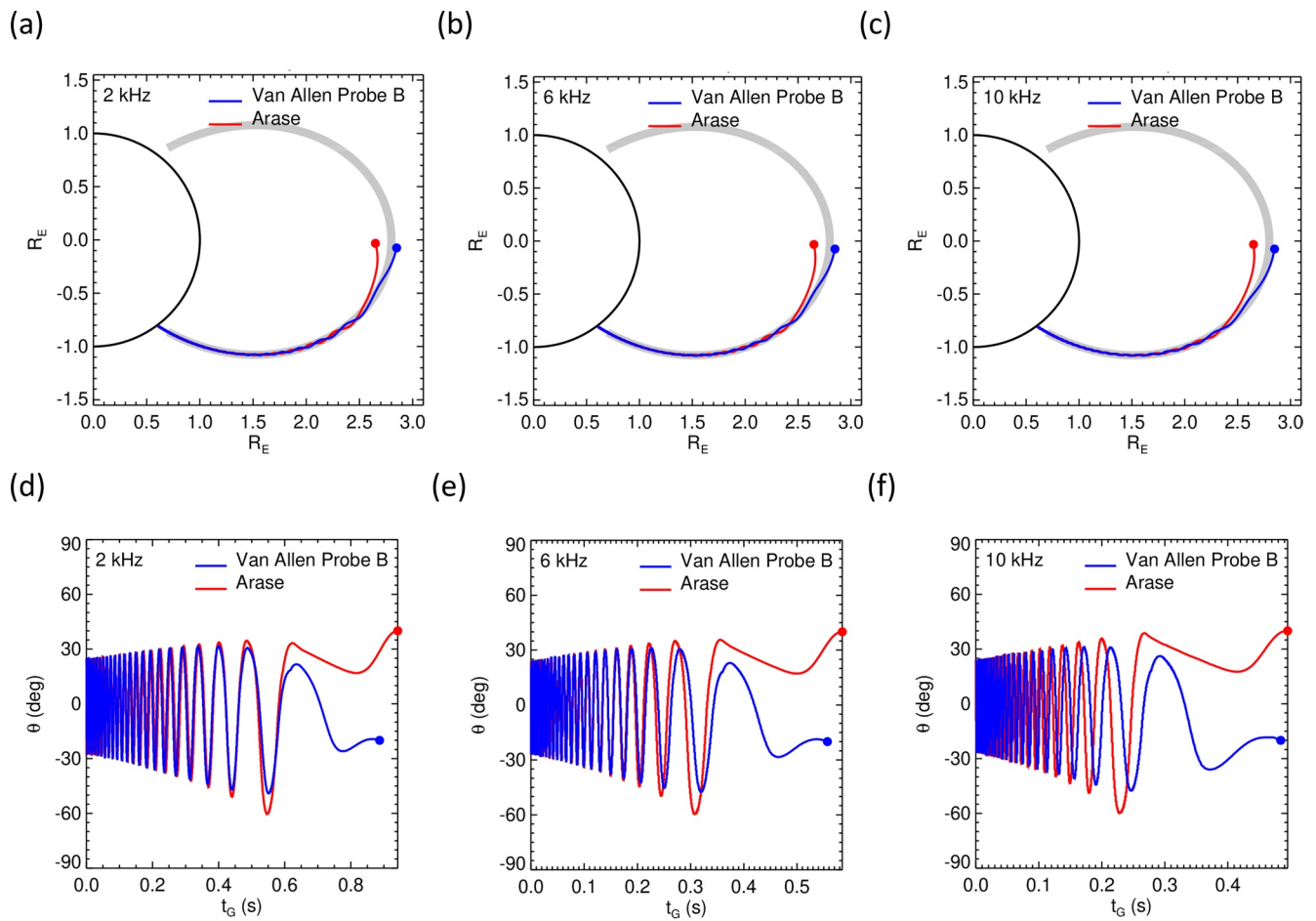


Figure 8. Backward ray tracing simulations from the locations of the (blue dot) Van Allen Probe B and (red dot) Arase spacecraft. (a–c) Color-coded projections of simulated rays on the plane of local magnetic meridian at magnetic local time of 16h for three selected frequencies of 2, 6, and 10 kHz; the density duct position and width are indicated by a thick gray line. (d–f) Angle of the wave vector from the local magnetic field line as a function of the simulated group time, for the same three frequencies, color-coded for the two spacecraft.

sufficient for ducting of the whistler mode waves at all five analyzed frequencies of 2, 4, 6, 8, and 10 kHz, representing the observed bandwidth of whistlers.

Figures 8a–8c show examples of results for three of these frequencies (2, 6, and 10 kHz). The blue-colored rays start at the location of the Van Allen Probe B spacecraft and the simulations are initialized using a wave vector inclined by 20° inward from the local field line and directed to the South. This corresponds to a direction antiparallel to a representative wave vector direction based on Figures 4c and 4d. The simulation then runs backward from the spacecraft to the source and the wave vector direction is updated during the accumulation of the group delay as it is shown in Figures 8d–8f. With a model exospheric temperature of 1,000 K, we needed to adjust the plasma density model to 70% of a measured value of $1,800 \text{ cm}^{-3}$ obtained by Van Allen Probe B from local measurements of the upper hybrid resonance frequency, in order to account for inaccuracies in the unknown density distribution along the duct. With this modified plasma density model, we have added the total group delays at the five simulated frequencies to the times of the two source return strokes, as they were obtained from the ground-based lightning location networks. The resulting times then fit well the observed whistlers as we demonstrate it by over plotted black squares in Figure 4.

The red-colored rays in Figures 8a–8c have been obtained using a similar simulation procedure but initialized at the position of the Arase spacecraft with a representative reverse wave vector inclined by 40° outward from the field line and directed to the South. The observed whistler traces in Figure 6 are again well reproduced by simulated group delays at five frequencies, added to the observed times of the source lightning

strokes, and represented by the over plotted black symbols in Figure 6. The best fit is obtained for a density model adjusted to 44% of a locally measured density of $3,600 \text{ cm}^{-3}$ on Arase (Kumamoto et al., 2018), owing again to inaccuracies of the model density distribution.

Our simple ray tracing simulation thus leads to a plausible explanation of the differences in the azimuth of the wave vector on the two spacecraft: As the observed wave vector angles are, at each analyzed frequency, below the Gendrin angle (which is between 57° and 84° on Van Allen Probe B and between 64° and 85° on Arase), the azimuth of the wave vector is the same as the azimuth of the Poynting vector (Gendrin, 1961; D. A. Gurnett & Bhattacharjee, 2012). Then, for a duct located between the two spacecraft, Arase must observe inward inclined wave vectors, being located closer to the Earth than the duct, and Van Allen Probe B should observe outward inclination of the wave vector, in order for the waves to reach the spacecraft located farther out from the Earth than the duct. Therefore, the waves propagate from their source lightning in the duct, they reflect back and forth from its plasma density gradient (see Figures 8d–8f), still fulfilling the WKB approximation with wavelengths of several km, until they can escape from it in a lower density region, reaching both receiving spacecraft.

The two source lightning strokes were independently time tagged by ground-based lightning detection networks. WWLLN has an absolute timing accuracy of $50 \mu\text{s}$ (Jacobson et al., 2006), while the GLD360 network has a timing accuracy of $10\text{--}60 \mu\text{s}$ (Said & Nag, 2014). Together with the above-described ray tracing analysis, this allows us to verify the correctness of the time tags attributed to measurements of the Van Allen Probe B and Arase spacecraft. The experimental time resolution of the dispersed whistler traces, resulting from the frequency-time analysis of their measured waveforms allows us to confirm that the time tags on both spacecraft correspond to UT with an uncertainty better than approximately 10 ms. This value is consistent with the average slope of the observed whistler trace of approximately $-100 \text{ Hz}/10 \text{ ms}$, characteristic for frequencies around 3 kHz. The uncertainty below 10 ms is also consistent with the observed times of peaks in whistler intensities at five analyzed frequencies in Figures 4 and 6, compared to the theoretical times of arrival of signals at these frequencies, derived from the measured time of source lightning discharge and simulated group delays (overplotted in Figures 4 and 6). The root-mean-square values of the five differences between the theoretical and experimental times of arrival are 7.2 ms for Van Allen Probe B and 4.3 ms for Arase.

6. Discussion on the Differences of Obtained Electric Field Amplitudes

We have shown that the analyzed whistlers indeed propagated along very similar paths (Figure 8) from their independently identified source strokes to both Arase and Van Allen Probe B. The final escape from the duct to different directions represents only a small part of the propagation path and did not cause differences of the observed amplitudes of the magnetic field fluctuations on the two spacecraft (Figure 7). The remaining unexplained observation of approximately twice larger amplitudes of the electric field measurements on Arase compared to the results from Van Allen Probe B can be hypothetically related to differences in wave vector directions measured by the two spacecraft. Higher inclinations of the wave vector from the direction of the background magnetic field, as they are observed on Arase, imply a higher ratio of the amplitude of electric field fluctuations to the amplitude of magnetic field fluctuations (E/B) carried by the whistler mode waves. The cold plasma theory (Stix, 1992; D. A. Gurnett & Bhattacharjee, 2012) together with the measured wave vector directions and plasma density should be sufficient to estimate these effects. However, this theory indicates the inability of differences in wave vector angles to explain the observations: estimated E/B ratios on Arase and Van Allen Probe B are 3.1% and 3.7% of the light speed, respectively. This result shows a small difference of obtained E/B ratios, which are even lower on Arase than on Van Allen Probe B, owing to a larger plasma density that was locally measured on Arase.

The different observed electric field amplitudes can be also explained by differences in the measured components of the fluctuating electric field vector: as we only use measurements by antennas in the spin plane of the two spacecraft, differences in the directions of the spin axis might cause that different 2D projections of the same electric field are measured on each spacecraft. A rough estimate of this possible effect relies on the attitude control strategy of both spacecraft: their spin axis was kept within 20° from the sunward direction, causing the maximum difference of electric field amplitudes by a factor of ~ 1.3 (2.3 dB), which is not

sufficient to explain the observations. The situation gets more complex if the electric field has a different polarization on the two spacecraft. The cold plasma theory (Stix, 1992) predicts for the measured plasma densities and wave vector directions, and for the frequency band from Figure 7, that the ellipticity of the electric field polarization should be similar on the two spacecraft: around 0.7 on Arase, and 0.9 on Van Allen Probe B.

Finally, the observed differences of the electric field measurements can be explained by a mismatch in calibration of the signals from the electric field sensors, linked to variations of the antenna-plasma impedances as a function of the density of the surrounding plasma medium. Preliminary results of a refined analysis based on the technique of Hartley et al. (2017) show that, for the measured density of $1,800 \text{ cm}^{-3}$ and for a frequency of 6 kHz (as in Figure 7), the Van Allen Probes spin plane antennas give smaller electric field amplitudes, by a factor $C_V \approx 0.84$ with respect to the correct amplitude of fluctuations of the ambient electric field. Similarly, a new technique of Matsuda, Kojima et al. (2021) shows that the Arase electric antennas, for the measured plasma density of $3,600 \text{ cm}^{-3}$, yield higher amplitudes with respect to the correct value by a factor $C_A \approx 1.3$. These corrections are not included in Figures 4–7, in which we use the currently archived Level 2 data from both spacecraft, calibrated using the amplitude and phase transfer functions which depend on frequency but not on the ambient plasma density.

A combination of both these corrections gives a factor of $C_A/C_V = 1.55$ that we should expect between the measured Van Allen Probe B and Arase electric field amplitudes. This correction brings the observed amplitudes from twice lower values on Van Allen Probe B compared to Arase to a factor of only $C_A/(2C_V) = 0.77$. The amplitudes therefore match within a 33% uncertainty (2.5 dB), which could be further linked to the above-discussed differences in attitude of the two spacecraft.

7. Conclusions

Using a fortuitous case of conjugate observation of strong whistlers by the Van Allen Probe B EMFISIS Waves instrument and by the Arase PWE instrument, we succeeded to compare measurements of electromagnetic waves by the two instruments with the following conclusions:

1. Magnetic field search coil measurements are well inter-calibrated within 30% for power spectral densities (1.2 dB), corresponding to a 14% precision of the amplitude inter-calibration
2. Currently archived electric field measurements show by a factor of 4 larger values of power spectral densities, corresponding to twice larger amplitudes on Arase compared to Van Allen Probes. This difference decreases down to an uncertainty of 33% (2.5 dB) once the most recent results on the antenna-plasma interactions are taken into account for both spacecraft. Corrections of measurements of the electric field fluctuations for the antenna-plasma impedance should be therefore added to the calibration procedures in the future
3. The polarization and propagation parameters have been determined from multicomponent measurement of electromagnetic field fluctuations and from determination of mutual phases and coherences between the measured components on each spacecraft. These parameters compose a consistent picture based on ducted propagation of whistler waves in a small plasma density enhancement, which is below the resolution of density measurements, and which is localized along the magnetic flux tube passing between the two spacecraft. The waves escape from this duct in the equatorial region with wave vectors inclined to both inward and outward directions, reaching the Arase and Van Allen Probe B spacecraft, respectively. The consistency of this pattern validates the inter-calibration of the multicomponent measurements on both spacecraft
4. Convincing link of observed whistlers to the records of two different ground-based lightning localization networks completes the above-described propagation scenario. It also allowed us to independently confirm the correctness of the Universal Time tagging of waveform measurements by both the EMFISIS Waves on the Van Allen Probe B spacecraft and the PWE instrument on the Arase spacecraft, with an uncertainty better than 10 ms

Data Availability Statement

The science data supporting the conclusions of the article were obtained from the EMFISIS site at the University of Iowa, <https://emfisis.physics.uiowa.edu/data/index>, and from the ERG Science Center (Miyoshi, Hori et al., 2018) operated by ISAS/JAXA and ISEE/Nagoya University, <https://ergsc.isee.nagoya-u.ac.jp/index.shtml.en>. The authors have used Van Allen Probes EMFISIS WFR waveform continuous burst level 2 data version 1.6.3 (probe A) and 1.6.2 (probe B), calibrated according to https://emfisis.physics.uiowa.edu/Waveform_Calibration/, spectral matrix data version 1.6.5 (probe A) and 1.6.4 (probe B), and magnetometer level 2 data version 1.6.1. The Arase PWE/WFC data are v00_02 (electric field, Kasahara, Kojima, Matsuda, Shoji, et al., 2020, magnetic field, Kasahara, Kojima, Matsuda, Ozaki, et al., 2020), MGF magnetic field data are level-2 v03.04 (Matsuoka, Teramoto, Imajo, et al., 2018), and orbit data are level-2 v03 (Miyoshi, Shinohara, & Jun, 2018). List of conjunctions of Arase and Van Allen Probes is available from <https://ergsc.isee.nagoya-u.ac.jp/mw/index.php/ErgGround/ErgVAPs>. The GLD360 data are available for sale from <https://www.vaisala.com/en/products/systems/lightning/gld360>. The WWLLN data are available for sale from the University of Washington (<http://wwlln.net/>).

Acknowledgments

The authors sincerely thank all our colleagues from both the Arase PWE and Van Allen Probes EMFISIS instrument teams for their valuable contributions to the instrument design, manufacturing, and testing. The authors thank Vaisala meteorologist Levi Blanchette for providing us with the GLD360 data. This study is supported by GACR grant 20-09671S, JSPS-KAKENHI (15H05815, 16H06286, 17H06140, 20H01959, 20K14546, 21H04520), JSPS-CAS bilateral project (JPJSBP120192504, JSPS-19-05), by the European Regional Development Fund-Project CREAT (C.Z.02.1.01/0.0/0.0/15_003/0000481), and by the joint research program of the Institute for Space-Earth Environmental Research, Nagoya University. This project has received funding from the European Union's Horizon 2020 research and innovation programme under grant agreement No. 870452 (PAGER). D. P. H. acknowledges support from NASA grant 80NSSC21K0519. The research at the University of Iowa is supported by JHU/APL through contract No. 921647 under NASA's prime contract No. NAS5-01072.

References

Bonnell, J. W., Mozer, F. S., Delory, G. T., Hull, A. J., Ergun, R. E., Cully, C. M., et al. (2008). The Electric Field Instrument (EFI) for THEMIS. *Space Science Reviews*, 141, 303–341. <https://doi.org/10.1007/s11214-008-9469-2>

Cerisier, J. (1970). Propagation perpendiculaire au voisinage de la fréquence de la résonance hybride basse. In *Plasma waves in space and in the laboratory* (Vol. 2, pp. 487–521). Edinburgh, UK: Edinburgh University Press.

Colpitts, C., Miyoshi, Y., Kasahara, Y., Delzanno, G. L., Wygant, J. R., Cattell, C. A., et al. (2020). First direct observations of propagation of discrete chorus elements from the equatorial source to higher latitudes, using the Van Allen Probes and Arase satellites. *Journal of Geophysical Research: Space Physics*, 125, e2020JA028315. <https://doi.org/10.1029/2020JA028315>

Cornilleau-Wehrin, N., Chanteur, G., Perraut, S., Rezeau, L., Robert, P., Roux, A., et al. (2003). First results obtained by the Cluster STAFF experiment. *Annales Geophysicae*, 21, 437–456. <https://doi.org/10.5194/angeo-21-437-2003>

Cornilleau-Wehrin, N., Chauveau, P., Louis, S., Meyer, A., Nappa, J. M., Perraut, S., et al. (1997). The Cluster Spatio-Temporal Analysis of Field Fluctuations (STAFF) Experiment. *Space Science Reviews*, 79, 107–136. <https://doi.org/10.1023/A:1004979209565>

Cummins, K. L. (2000). Continental-scale detection of cloud-to-ground lightning. *IEEE Transactions on Power and Energy*, 120(1), 2–5. https://doi.org/10.1541/ieejpes1990.120.1_2

Gendrin, R. (1961). Le guidage des whistlers par le champ magnetique. *Planetary and Space Science*, 5, 274–278. [https://doi.org/10.1016/0032-0633\(61\)90096-4](https://doi.org/10.1016/0032-0633(61)90096-4)

Gurnett, D., & Kurth, W. (2008). Intense plasma waves at and near the solar wind termination shock. *Nature*, 454, 78–80. <https://doi.org/10.1038/nature07023>

Gurnett, D., Kurth, W., Roux, A., Bolton, S. J., & Kennel, C. F. (1996). Evidence for a magnetosphere at Ganymede from plasma-wave observations by the Galileo spacecraft. *Nature*, 384, 535–537. <https://doi.org/10.1038/384535a0>

Gurnett, D., Kurth, W., & Scarf, F. (1981). Narrowband electromagnetic emissions from Saturn's magnetosphere. *Nature*, 292, 733–737. <https://doi.org/10.1038/292733a0>

Gurnett, D., Kurth, W., & Scarf, F. (1983). Narrowband electromagnetic emissions from Jupiter's magnetosphere. *Nature*, 302, 385–388. <https://doi.org/10.1038/302385a0>

Gurnett, D., Shawhan, S., & Pfeiffer, G. (1966). Hook whistler—A new equatorial whistler observed by Injun 3. *Nature*, 212, 1442–1443. <https://doi.org/10.1038/2121442a0>

Gurnett, D. A., & Bhattacharjee, A. (2012). *Introduction to plasma Physics with space and laboratory applications*. Cambridge University Press. <https://doi.org/10.1017/CBO9780511809125>

Gurnett, D. A., Persoon, A. M., Randall, R. F., Odem, D. L., Remington, S. L., Averkamp, T. F., et al. (1995). The Polar plasma wave instrument. *Space Science Reviews*, 71, 597–622. <https://doi.org/10.1007/BF00751343>

Hartley, D. P., Kletzing, C. A., Kurth, W. S., Hospodarsky, G. B., Bounds, S. R., Averkamp, T. F., et al. (2017). An improved sheath impedance model for the Van Allen Probes EFW instrument: Effects of the spin axis antenna. *Journal of Geophysical Research: Space Physics*, 122, 4420–4429. <https://doi.org/10.1002/2016JA023597>

Hartley, D. P., Kletzing, C. A., Santolik, O., Chen, L., & Horne, R. B. (2018). Statistical properties of plasmaspheric hiss from Van Allen Probes observations. *Journal of Geophysical Research: Space Physics*, 123, 2605–2619. <https://doi.org/10.1002/2017JA024593>

Horne, R. B., Thorne, R. M., Shprits, Y. Y., Meredith, N. P., Glauert, S. A., Smith, A. J., et al. (2005). Wave acceleration of electrons in the Van Allen radiation belts. *Nature*, 437(7056), 227–230. <https://doi.org/10.1038/nature03939>

Hutchins, M. L., Holzworth, R. H., Brundell, J. B., & Rodger, C. J. (2012). Relative detection efficiency of the World Wide Lightning Location Network. *Radio Science*, 47, RS6005. <https://doi.org/10.1029/2012RS005049>

Hutchins, M. L., Holzworth, R. H., Rodger, C. J., & Brundell, J. B. (2012). Far-field power of lightning strokes as measured by the World Wide Lightning Location Network. *Journal of Atmospheric and Oceanic Technology*, 29, 1102–1110. <https://doi.org/10.1175/JTECH-D-11-00174.1>

Jacobson, A. R., Holzworth, R., Harlin, J., Dowden, R., & Lay, E. (2006). Performance assessment of the World Wide Lightning Location Network (WWLLN), using the Los Alamos Sferic Array (LASA) as ground truth. *Journal of Atmospheric and Oceanic Technology*, 23(8), 1082–1092. <https://doi.org/10.1175/JTECH1902.1>

Kasaba, Y., Ishisaka, K., Kasahara, Y., Imachi, T., Yagitani, S., Kojima, H., et al. (2017). Wire Probe Antenna (WPT) and Electric Field Detector (EFD) of Plasma Wave Experiment (PWE) aboard the Arase satellite: Specifications and initial evaluation results. *Earth, Planets, and Space*, 69, 174. <https://doi.org/10.1186/s40623-017-0760-x>

Kasahara, Y., Kasaba, Y., Kojima, H., Yagitani, S., Ishisaka, K., Kumamoto, A., et al. (2018). The Plasma Wave Experiment (PWE) on board the Arase (ERG) satellite. *Earth, Planets, and Space*, 70, 86. <https://doi.org/10.1186/s40623-018-0842-4>

- Kasahara, Y., Kojima, H., Matsuda, S., Ozaki, M., Yagitani, S., Shoji, M., et al. (2020). *The PWE/WFC instrument Level-2 magnetic field waveform data of Exploration of energization and Radiation in Geospace (ERG) Arase satellite*, ERG-Science Center. Institute for Space-Earth Environmental Research, Nagoya University. <https://doi.org/10.34515/DATA.ERG-09001>
- Kasahara, Y., Kojima, H., Matsuda, S., Shoji, M., Nakamura, S., Kitahara, M., et al. (2020). *The PWE/WFC instrument Level-2 electric field waveform data of Exploration of energization and Radiation in Geospace (ERG) Arase satellite*, ERG-Science Center. Institute for Space-Earth Environmental Research, Nagoya University. <https://doi.org/10.34515/DATA.ERG-09000>
- Kletzing, C., Kurth, W. S., Acuna, M., MacDowall, R. J., Torbert, R. B., Averkamp, T., et al. (2013). The Electric and Magnetic Field Instrument Suite and Integrated Science (EMFISIS) on RBSP. *Space Science Reviews*, 179, 127–181.
- Kumamoto, A., Tsuchiya, F., Kasahara, Y., Kasaba, Y., Kojima, H., Yagitani, S., et al. (2018). High-Frequency Analyzer (HFA) of Plasma Wave Experiment (PWE) onboard the Arase spacecraft. *Earth, Planets, and Space*, 70, 82. <https://doi.org/10.1186/s40623-018-0854-0>
- Kurth, W. S., De Pascuale, S., Faden, J. B., Kletzing, C. A., Hospodarsky, G. B., Thaller, S., & Wygant, J. R. (2015). Electron densities inferred from plasma wave spectra obtained by the Waves Instrument on Van Allen Probes. *Journal of Geophysical Research: Space Physics*, 120, 904–914. <https://doi.org/10.1002/2014JA020857>
- Matsuda, S., Kasahara, Y., Kojima, H., Kasaba, Y., Yagitani, S., Ozaki, M., et al. (2018). Onboard software of plasma wave experiment aboard Arase: Instrument management and signal processing of waveform capture/onboard frequency analyzer. *Earth, Planets, and Space*, 70, 75. <https://doi.org/10.1186/s40623-018-0838-0>
- Matsuda, S., Kojima, H., Kasahara, Y., Kasaba, Y., Kumamoto, A., Tsuchiya, F., et al. (2021). Direct antenna impedance measurement for quantitative AC electric field measurement by Arase. *Journal of Geophysical Research: Space Physics*, 126, e2021JA029111. <https://doi.org/10.1029/2021JA029111>
- Matsuda, S., Miyoshi, Y., Nakamura, S., Kitahara, M., Shoji, M., Hori, T., et al. (2021). ISEE_Wave: Interactive plasma wave analysis tool. *Earth, Planets, and Space*, 73, 110. <https://doi.org/10.1186/s40623-021-01430-3>
- Matsuoka, A., Teramoto, M., Imajo, S., Kurita, S., Miyoshi, Y., & Shinohara, I. (2018). *The MGF instrument Level-2 spin-averaged magnetic field data of Exploration of energization and Radiation in Geospace (ERG) Arase satellite*, ERG-Science Center. Institute for Space-Earth Environmental Research, Nagoya University. <https://doi.org/10.34515/DATA.ERG-06001>
- Matsuoka, A., Teramoto, M., Nomura, R., Nosé, M., Fujimoto, A., Tanaka, Y., et al. (2018). The ARASE(ERG) magnetic field investigation. *Earth, Planets, and Space*, 70, 43. <https://doi.org/10.1186/s40623-018-0800-1>
- Meredith, N. P., Horne, R. B., Kersten, T., Li, W., Bortnik, J., Sicard, A., & Yearby, K. H. (2018). Global model of plasmaspheric hiss from multiple satellite observations. *Journal of Geophysical Research: Space Physics*, 123, 4526–4541. <https://doi.org/10.1029/2018JA025226>
- Miyoshi, Y., Hori, T., Shoji, M., Teramoto, M., Chang, T.-F., Segawa, T., et al. (2018). The ERG Science Center. *Earth, Planets, and Space*, 70, 96. <https://doi.org/10.1186/s40623-018-0867-8>
- Miyoshi, Y., Shinohara, I., & Jun, C.-W. (2018). *The Level-2 orbit data of Exploration of energization and Radiation in Geospace (ERG) Arase satellite*, ERG-Science Center. Institute for Space-Earth Environmental Research, Nagoya University. <https://doi.org/10.34515/DATA.ERG-12000>
- Miyoshi, Y., Shinohara, I., Takashima, T., Asamura, K., Higashio, N., Mitani, T., et al. (2018). Geospace exploration project ERG. *Earth, Planets, and Space*, 70, 101. <https://doi.org/10.1186/s40623-018-0862-0>
- Mosier, S., & Gurnett, D. (1969). Ionospheric observation of VLF electrostatic noise related to harmonics of the proton gyrofrequency. *Nature*, 223, 605–606. <https://doi.org/10.1038/223605a0>
- Roux, A., Le Contel, O., Coillot, C., Bouabdellah, A., Porte, B., Alison, D., et al. (2008). The search coil magnetometer for THEMIS. *Space Science Review*, 141, 265–275. <https://doi.org/10.1007/s11214-008-9455-8>
- Rudlosky, S. D., Peterson, M. J., & Kahn, D. T. (2017). GLD360 performance relative to TRMM LIS. *Journal of Atmospheric and Oceanic Technology*, 34(6), 1307–1322. <https://doi.org/10.1175/JTECH-D-16-0243.1>
- Said, R. K., Inan, U., & Cummins, K. (2010). Long-range lightning geolocation using a VLF radio atmospheric waveform bank. *Journal of Geophysical Research*, 115, 1–19. <https://doi.org/10.1029/2010JD013863>
- Said, R. K., & Nag, A. (2014). *Method to Improve Location Accuracy of the GLD360*. 23rd International Lightning Detection Conference and 5th International Lightning Meteorology conference, Tucson, Arizona, USA.
- Santolík, O., Chum, J., Parrot, M., Gurnett, D. A., Pickett, J. S., & Cornilleau-Wehrin, N. (2006). Propagation of whistler mode chorus to low altitudes: Spacecraft observations of structured ELF hiss. *Journal of Geophysical Research*, 111, A10208. <https://doi.org/10.1029/2005JA011462>
- Santolík, O., Hospodarsky, G. B., Kasahara, Y., Pickett, J. S., Kurth, W. S., Matsuda, S., et al. (2018). Multi-point measurements and ray-tracing simulations of chorus wave packets. AGU Fall Meeting. Retrieved from <https://agu.confex.com/agu/fm18/meetingapp.cgi/Paper/405459>
- Santolík, O., Parrot, M., Inan, U. S., Burešová, D., Gurnett, D. A., & Chum, J. (2009). Propagation of unducted whistlers from their source lightning: A case study. *Journal of Geophysical Research*, 114, A03212. <https://doi.org/10.1029/2008JA013776>
- Santolík, O., Parrot, M., & Lefeuvre, F. (2003). Singular value decomposition methods for wave propagation analysis. *Radio Science*, 38(1), 1010. <https://doi.org/10.1029/2000RS002523>
- Santolík, O., Pickett, J. S., Gurnett, D. A., Menietti, J. D., Tsurutani, B. T., & Verkhoglyadova, O. (2010). Survey of Poynting flux of whistler mode chorus in the outer zone. *Journal of Geophysical Research*, 115, A00F13. <https://doi.org/10.1029/2009JA014925>
- Santolík, O., Pickett, J. S., Gurnett, D. A., & Storey, L. R. O. (2002). Magnetic component of narrowband ion cyclotron waves in the auroral zone. *Journal of Geophysical Research: Space Physics*, 107(A12), 1444. <https://doi.org/10.1029/2001JA000146>
- Stix, T. H. (1992). *Waves in plasmas*. New York: Springer.
- Storey, L. R. O. (1953). An investigation of whistling atmospherics. *Philosophical Transactions of the Royal Society of London. Series A, Mathematical and Physical Sciences* 246, 113–141. <https://doi.org/10.1098/rsta.1953.0011>
- Thorne, R., Li, W., Ni, B., Ma, Q., Bortnik, J., Chen, L., et al. (2013). Rapid local acceleration of relativistic radiation-belt electrons by magnetospheric chorus. *Nature*, 504, 411–414. <https://doi.org/10.1038/nature12889>
- Torbert, R. B., Russell, C. T., Magnes, W., Ergun, R. E., Lindqvist, P.-A., LeContel, O., et al. (2016). The FIELDS instrument suite on MMS: Scientific objectives, measurements, and data products. *Space Science Review* 199, 105–135. <https://doi.org/10.1007/s11214-014-0109-8>